

A PD-L1/EGFR bispecific antibody combines immune checkpoint blockade and direct anti-cancer action for an enhanced anti-tumor response

Laura Rubio-Pérez, Rodrigo Lázaro-Gorines, Seandean L. Harwood, Marta Compte, Rocío Navarro, Antonio Tapia-Galisteo, Jaume Bonet, Belén Blanco, Simon Lykkemark, Ángel Ramírez-Fernández, Mariola Ferreras-Gutiérrez, Carmen Domínguez-Alonso, Laura Díez-Alonso, Alejandro Segura-Tudela, Oana Hangiu, Ainhoa Erce-Llamazares, Francisco J. Blanco, Cruz Santos, José L. Rodríguez-Peralto, Laura Sanz & Luis Álvarez-Vallina

To cite this article: Laura Rubio-Pérez, Rodrigo Lázaro-Gorines, Seandean L. Harwood, Marta Compte, Rocío Navarro, Antonio Tapia-Galisteo, Jaume Bonet, Belén Blanco, Simon Lykkemark, Ángel Ramírez-Fernández, Mariola Ferreras-Gutiérrez, Carmen Domínguez-Alonso, Laura Díez-Alonso, Alejandro Segura-Tudela, Oana Hangiu, Ainhoa Erce-Llamazares, Francisco J. Blanco, Cruz Santos, José L. Rodríguez-Peralto, Laura Sanz & Luis Álvarez-Vallina (2023) A PD-L1/EGFR bispecific antibody combines immune checkpoint blockade and direct anti-cancer action for an enhanced anti-tumor response, *Oncolmmunology*, 12:1, 2205336, DOI: [10.1080/2162402X.2023.2205336](https://doi.org/10.1080/2162402X.2023.2205336)

To link to this article: <https://doi.org/10.1080/2162402X.2023.2205336>



© 2023 The Author(s). Published with license by Taylor & Francis Group, LLC.



[View supplementary material](#)



Published online: 24 Apr 2023.



[Submit your article to this journal](#)



[View related articles](#)



[View Crossmark data](#)

A PD-L1/EGFR bispecific antibody combines immune checkpoint blockade and direct anti-cancer action for an enhanced anti-tumor response

Laura Rubio-Pérez ^{a,b,c,d}, Rodrigo Lázaro-Gorines ^{a,b,c}, Seandean L. Harwood ^e, Marta Compte ^f, Rocío Navarro ^f, Antonio Tapia-Galisteo ^{a,b,c}, Jaime Bonet ^g, Belén Blanco ^{a,b,c}, Simon Lykkemark ^h, Ángel Ramírez-Fernández ^{a,b,c}, Mariola Ferreras-Gutiérrez ⁱ, Carmen Domínguez-Alonso ^{a,b,c}, Laura Díez-Alonso ^{a,b,c}, Alejandro Segura-Tudela ^{a,b,c}, Oana Hangiu ^{a,b,f}, Ainhoa Erce-Llamazares ^{a,b,f}, Francisco J. Blanco ⁱ, Cruz Santos ^j, José L. Rodríguez-Peralto ^{k,l,m,n}, Laura Sanz ^{n,o}, and Luis Álvarez-Vallina ^{a,b,c,d}

^aCancer Immunotherapy Unit (UNICA), Department of Immunology, Hospital Universitario 12 de Octubre, Madrid, Spain; ^bImmuno-Oncology and Immunotherapy Group, Instituto de Investigación Sanitaria 12 de Octubre (imas12), Madrid, Spain; ^cH120-CNIO Cancer Immunotherapy Clinical Research Unit, Spanish National Cancer Research Centre (CNIO), Madrid, Spain; ^dChair for Immunology UFV/Merck, Universidad Francisco de Vitoria (UFV), Madrid, Spain; ^eDepartment of Molecular Biology and Genetics, Aarhus University, Aarhus C, Denmark; ^fDepartment of Antibody Engineering, Leadartis SL, QUBE Technology Park, Madrid, Spain; ^gInstitute of Bioengineering, École Polytechnique Fédérale de Lausanne, Lausanne, Switzerland; ^hImmunotherapy and Cell Engineering Laboratory, Department of Engineering, Aarhus University, Aarhus C, Denmark; ⁱCentro de Investigaciones Biológicas Margarita Salas (CIB), CSIC, Madrid, Spain; ^jFaculty of Experimental Sciences, Universidad Francisco de Vitoria (UFV), Madrid, Spain; ^kDepartment of Pathology, Hospital Universitario 12 de Octubre, Madrid, Spain; ^lDepartment of Pathology, Universidad Complutense, Madrid, Spain; ^mCutaneous Oncology Group, Instituto de Investigación Sanitaria 12 de Octubre (imas12), Madrid, Spain; ⁿCentro de Investigación Biomédica en Red en Oncología (CIBERONC), Madrid, Spain; ^oMolecular Immunology Unit, Hospital Universitario Puerta de Hierro Majadahonda, Madrid, Spain

ABSTRACT

Immune checkpoint blockade (ICB) with antibodies has shown durable clinical responses in a wide range of cancer types, but the overall response rate is still limited. Other effective therapeutic modalities to increase the ICB response rates are urgently needed. New bispecific antibody (bsAb) formats combining the ICB effect and a direct action on cancer cells could improve the efficacy of current immunotherapies. Here, we report the development of a PD-L1/EGFR symmetric bsAb by fusing a dual-targeting tandem trimmer body with the human IgG1 hinge and Fc regions. The bsAb was characterized in vitro and the antitumor efficacy was evaluated in humanized mice bearing xenografts of aggressive triple-negative breast cancer and lung cancer. The IgG-like hexavalent bsAb, designated IgTT-1E, was able to simultaneously bind both EGFR and PD-L1 antigens, inhibit EGF-mediated proliferation, effectively block PD-1/PD-L1 interaction, and induce strong antigen-specific antibody-dependent cellular cytotoxicity activity in vitro. Potent therapeutic efficacies of IgTT-1E in two different humanized mouse models were observed, where tumor growth control was associated with a significantly increased proportion of CD8⁺ T cells. These results support the development of IgTT-1E for the treatment of EGFR⁺ cancers.

ARTICLE HISTORY

Received 2 January 2023
Revised 16 April 2023
Accepted 17 April 2023

KEYWORDS



Cancer immunotherapy, bispecific antibody; dual action; epithelial growth factor receptor; immune checkpoint blockade


Introduction

Modulating immune responses using monoclonal antibodies (mAbs) is one of the most promising approaches for cancer immunotherapy¹. Immune checkpoints are coinhibitory and costimulatory receptors that are crucial for maintaining self-tolerance and modulating immune responses². However, inhibitory checkpoints can be “hijacked” by tumors to evade immune responses³. MAb-based blockade of coinhibitory immune receptors, such as cytotoxic T lymphocyte antigen 4 (CTLA-4), programmed cell death-1 (PD-1) receptor, or PD-1 ligand (PD-L1) has shown durable tumor clinical responses in a wide range of cancer types, but their efficacy is limited to 10% to 30% of patients⁴. Different factors, such as the tumor mutational burden and immunogenicity of cancer cells, the composition of the tumor microenvironment (TME) and the degree of immune cell infiltration, influence the response to immune

checkpoint blockade (ICB)⁵. Increasing the response rates to ICB is likely to require the design of therapeutic combinations that are tailored to the aforementioned factors⁶. On the other hand, EGFR is a receptor tyrosine kinase well-known as a tumor-associated antigen (TAA) with an important functional role, since EGFR deregulation promotes proliferation, apoptosis inhibition and invasion of cancer cells⁷. Therefore, mAb targeting EGFR not only mark tumor cells for immune killing but also may inhibit phosphorylation of key intracellular tyrosine residues, thus preventing ligand-mediated mitogenic signaling⁸.

As of January 2023, seven immune checkpoint blockers (ICB) preventing PD1/PD-L1 interaction had been approved for clinical use by the Food and Drug Administration (FDA) and the European Medicines Agency (EMA), and six others are in regulatory review, being *atezolizumab* the first anti-PD-L1

CONTACT Luis Álvarez-Vallina  lav.imas12@h12o.es  Cancer Immunotherapy Unit (UNICA), Department of Immunology, Hospital Universitario 12 de Octubre, Avda. Córdoba s/n, Madrid 28041, Spain

 Supplemental data for this article can be accessed online at <https://doi.org/10.1080/2162402X.2023.2205336>

© 2023 The Author(s). Published with license by Taylor & Francis Group, LLC.

This is an Open Access article distributed under the terms of the Creative Commons Attribution-NonCommercial License (<http://creativecommons.org/licenses/by-nc/4.0/>), which permits unrestricted non-commercial use, distribution, and reproduction in any medium, provided the original work is properly cited. The terms on which this article has been published allow the posting of the Accepted Manuscript in a repository by the author(s) or with their consent.

mAb in the market (2017). With respect to EGFR, three conventional mAbs [*cetuximab*, *panitumumab* –both approved for colorectal cancer (CRC)- and *nectinumab* –for non-small cell lung cancer (NSCLC)- and the bispecific antibody (bsAb) *amivantamab* (EGFR x c-MET, for NSCLC with EGFR exon 20 insertion mutations) are currently in the market. Antibody therapeutics that are approved for marketing in regions other than the US or EU include two anti-EGFR (*nimotuzumab* and *cetuximab* conjugated to the photosensitizer IR700) and seven anti-PD1⁹.

Designing agents that combine the immunomodulatory effect of an ICB and a direct action on cancer cells could open new perspectives in cancer immunotherapy. Here, we generated a novel PD-L1/EGFR bispecific antibody (bsAb) by fusing a dual-targeting tandem trimerbody (TT)¹⁰ with the human IgG1 hinge and Fc regions. The TT format has been previously described and is a single-chain fusion of three single-domain V_{HH} antibodies with three collagen XVIII trimerization domains (TIE)^{8–10}, with intercalating glycine-serine-based linkers. Each V_{HH} is encoded separately, allowing mono-, bi-, and tri-specific molecules to be produced⁷. Here, the first V_{HH} was replaced by a PD-L1-specific scFv, and an EGFR-specific V_{HH} was used in the second and third V_{HH} positions. The resulting IgG-like hexavalent bsAb, designated IgTT-1E, simultaneously bound both targeted antigens, inhibited EGF-mediated proliferation, effectively blocked PD-1/PD-L1 interaction and induced potent antigen-specific antibody-dependent cellular cytotoxicity (ADCC) activity *in vitro*. A potent therapeutic effect of IgTT-1E was observed in humanized mice bearing aggressive EGFR⁺PD-L1⁺ human triple-negative breast cancer (TNBC) and lung cancer cell-line – derived xenografts (CDX). These data provide a promising basis for the further clinical development of IgTT-1E and similarly designed symmetric antibodies against different targets.

Materials and methods

Cell lines and culture conditions

HEK-293 (CRL-1573), A431 (CRL-1555), NIH/3T3 (CRL-1658), MDA-MB-231 (HTB-26) and CHO-K1 (CCL-61) cells were cultured in Dulbecco's modified Eagle's medium (DMEM) (Life Technologies, cat# 10313021) supplemented with 2 mmol/l L-glutamine, 10% (v/v) heat-inactivated fetal bovine serum (FBS) (Merck Life Science, cat# F7524-500 ML), and antibiotics (100 units/mL penicillin, 100 mg/mL streptomycin; both from Life Technologies) at 37 °C in 5% CO₂ humidity. A549 (CCL-185) cells were cultured in RPMI-1640 (Lonza, cat# 12-702Q) supplemented with 2 mmol/l L-glutamine, 10% (v/v) heat-inactivated FBS, and antibiotics. All these cell lines were obtained from the American Type Culture Collection. NIH/3T3 cells expressing human EGFR (3T3^{EGFR}) were kindly provided by Dr. A. Villalobo [Instituto de Investigaciones Biomédicas "Alberto Sols". IIBm (CSIC-UAM), Madrid, Spain]. Jurkat T cells stably expressing human PD-1 and NFAT-induced luciferase (Jurkat^{NFAT-RE-luc/PD-1}) and CHO-K1 cells stably expressing human PD-L1 (PD-L1 aAPC/CHO-K1), were obtained from Promega (cat# J1250). CHO-K1 cells stably expressing

human PD-L1 (CHO^{PD-L1}) were obtained from Genlantis (xCELLerateTM PD-L1 Stable Cell Line, XCL-PDL1) and CHO-K1 cells stably expressing human EGFR (CHO^{EGFR}), or both (CHO^{EGFR-PD-L1}) were generated using human EGFR encoding commercial lentiviral particles (G&P Biosciences, cat# LTV0169). All cell lines were routinely screened for mycoplasma contamination by PCR using the Mycoplasma PlusTM Primer Set (Biotools B&M Labs, cat# 90022).

Construction of expression vectors

The plasmid pCR3.1-FLAG/Strep-αEGFR₃-TIE-αCD3 was generated by cloning the insert OncoM-FLAG/Strep-αEGFR flanked by *HindIII-NotI* (GeneArt AG, Thermo Fischer) into the plasmid pCR3.1-αEGFR₃-TIE-αCD3 encoding the bispecific EGFR x anti-CD3 ATTACK¹¹. Then, the FLAG/Strep-αEGFR V_{HH}-based tandem trimerbody (TT) was subcloned as *HindIII/BamHI* into pCR3.1-hFc-His vector containing a human IgG₁ hinge and Fc region, resulting in pCR3.1-FLAG/Strep-αEGFR₃-hFc-His (IgTT-E). To generate the PD-L1/EGFR bispecific IgTT (IgTT-1E) expressing vector, the OncoM-FLAG/Strep-αPD-L1 fragment flanked by *HindIII-NotI* (GeneArt AG) was cloned into the plasmid pCR3.1-FLAG/Strep-αEGFR₃-hFc-His. All the sequences were verified using primers FwCMV and RvBGH oligonucleotides (Table S1).

Expression and purification of recombinant antibodies

HEK-293 cells were transfected with the appropriated vectors by Lipofectamine 3,000 transfection kit (Fisher Scientific, cat# 15292465) and selected in complete DMEM supplemented with 500 µg/ml of G418 to generate stable cell lines. Conditioned media were collected and processed using Strep-Tactin purification system (IBA Lifesciences) in an ÄKTA Prime plus system (Life Technologies). The purified antibodies were dialyzed overnight at 4 °C against PBS pH 7.4 supplemented with 150 mM NaCl and analyzed by sodium dodecyl sulfate (SDS)-polyacrylamide gel electrophoresis (PAGE) under reducing conditions.

Western blotting

Protein samples were analyzed by mean of 10–20% Tris-glycine SDS-PAGE under reducing conditions, transferred onto nitrocellulose membranes (Thermo Fisher Scientific, cat# IB23002) and probed with mouse anti-FLAG IgG₁ (clone M2, Sigma-Aldrich, cat# F3165) (1 µg/ml), followed by incubation with HRP-conjugated goat anti-mouse IgG (GAM-HRP) (1:10,000 dilution) (Sigma, cat# A2554). Visualization of protein bands was performed with Pierce ECL Plus Western Blotting Substrate (Thermo Scientific, cat# 32132), using ChemiDoc MP Imaging System and Image Lab software (both from BioRad).

Enzyme-linked immunosorbent assay

The human EGFR-Fc (EGFR-Fc, R&D Systems, cat# 344-ER) or human PD-L1-Fc (PD-L1-Fc, Peprotech, cat# 310-35)

chimeras were immobilized (2.5 µg/ml in PBS) on Maxisorp 96-well plates (NUNC Brand Products, cat# 44240) overnight at 4°C. After washing and blocking, conditioned media or purified protein solution (1 µg/ml) was added and incubated for 1 hour at room temperature. The wells were washed and HRP-conjugated anti-poly Histidine (Sigma-Aldrich, cat# A7058), HRP-conjugated anti-FLAG (M2 clone, Sigma-Aldrich, cat# A8592), mouse anti-Myc (clone 9E10, Millipore, cat# 05-419) or HRP-conjugated goat anti-human IgG (GAH) (Sigma-Aldrich, cat# A0170) were added (1 µg/ml). After washing, in the case of mouse anti-Myc, GAM-HRP (1:2,000 dilution) (Jackson ImmunoResearch, cat# 115-085-166) was added for 1 hour at room temperature. Finally, after washing, the plate was developed using 100 µl 3,3',5,5'-tetramethylbenzidine (TMB) (Sigma-Aldrich, cat# T0440) and stopped by 100 µl of 1 N H₂SO₄. Absorbance was read at 450–620 nm using Multiskan FC photometer (Thermo Scientific).

Size exclusion chromatography-multiangle light scattering

The experiments were performed on a Superdex 200 Increase 10/300 GL column (Cytiva) attached in-line to a DAWN EOS light scattering photometer (Wyatt Technology) and an ultraviolet light absorbance detector (ThermoFinnigan SpectraSYSTEM UV2000). The chromatography was run at room temperature and the scattering detector was thermostated at 23 °C. The column was equilibrated with running buffer (PBS pH 7.4 plus 150 mM NaCl, 0.1 µm filtered) and the size exclusion chromatography-multiangle light scattering (SEC-MALS) system was calibrated with a sample of BSA (Albumin, Monomer bovine, Sigma-Aldrich, cat#A1900) at 2 mg/ml in the same buffer. 230 µl of the antibody solutions at 0.3 or 0.4 mg/ml were injected into the column at a flow rate of 0.5 ml/min. The column has an exclusion volume of 8.6 ml, and no absorbance (no aggregated proteins) was observed in the chromatograms at this volume. Data acquisition and analysis were performed using ASTRA software (Wyatt Technology). The reported molar masses correspond to the center of the chromatography peaks. Based on numerous measurements on BSA samples under similar conditions the estimation of the experimental error in the molar mass is around 5%.

Molecular Modeling

The IgTT-E three-dimensional representation was built by homology modeling using MODELLER¹². Two templates were combined to generate the model, the V_{HH}-based mono-specific TT was built using as template the anti-CEA TT constructed in a previous work¹³, while the Fc domain was based on the human IgG1 B12 structure (pdb:1HZH.H)¹⁴, obtained from the Protein Data Bank¹⁵. The Fc template was obtained with BLAST¹⁶; with an e-value of 1e-169 and a 99% of sequence identity for the domain. The structure of 1HZH was also used to guide dimerization. The IgTT-1E model was built by combining the IgTT-E model and the interleukin 18 receptor antagonist scFv (pdb:6NK9.D)¹⁷ for the anti-PD-L1

scFv domain. The template was obtained through BLAST with an e-value of 2e-138 and 83% of sequence identity for the domain.

Biolayer interferometry

The binding of the IgTT-E to immobilized EGFR-Fc, and of the IgTT-1E to immobilized EGFR-Fc and PD-L1-Fc was measured using biolayer interferometry (BLI) on an Octet RED96 system (Fortebio). The binding to EGFR was compared to that of *cetuximab* (ctx) (Merck KGaA, Darmstadt, Germany), and the binding to PD-L1 was compared with *atezolizumab* (atz) (Fritz Hoffmann-La Roche, Basel, Switzerland). Both antigens were immobilized onto AR2G biosensors (Fortebio) at pH 5.0 using amine reactive coupling. Antibodies in HEPES-buffered saline (HBS; 20 mM HEPES, 150 mM NaCl, pH 7.4) at 10 nM were associated with either immobilized antigen for 30 minutes, after which the dissociation of antibody from the biosensor was measured for 30 minutes in HBS buffer only. After the IgTT-1E and ctx had bound to immobilized EGFR, bispecific binding to PD-L1-Fc in solution was then investigated by the subsequent treatment of the biosensors with 20 nM of PD-L1-Fc in HBS for 30 minutes. To determine binding kinetics to immobilized EGFR and PD-L1, the Octet Data Analysis (Fortebio) software was used to fit the experiment data to a 1:1 binding model with an asymptotic association phase and an exponential decay dissociation phase and regression to the chi² value.

Serum stability

Purified IgTT-1E was incubated in 60% (v/v) human serum (Sigma-Aldrich, cat# H4522) at 37°C for 96 hours. The binding activity of the sample at 0 time point was set as 100% to calculate the corresponding decay in PD-L1 and EGFR binding by enzyme-linked immunosorbent assay (ELISA). Samples were analyzed with Multiskan FC Photometer and GraphPad Prism software. Results correspond to one experiment performed in triplicate.

Flow cytometry

CHO^{EGFR} or CHO^{PD-L1} cells (1 × 10⁵ cells/well) were incubated for 1 hour on ice with purified antibodies (6.67 nM), washed and incubated for 30 minutes with a PE-conjugated F(ab')₂ GAH IgG antibody (Jackson ImmunoResearch, cat# 109-116-170). *Trastuzumab* (tra) (Fritz Hoffmann-La Roche), atz and ctx (6.67 nM) were used as controls. After washing, DAPI (Sigma Aldrich, cat# D9542) was added and samples were analyzed with FACSCanto II Flow Cytometer (Becton Dickinson).

Inhibition of EGFR-mediated cell proliferation and signaling

A431 cells were seeded in complete DMEM in 96-well plates. After 24 hours, the medium was replaced by DMEM 1% FBS containing equimolar concentrations (0.19–50 nM) of ctx, atz, IgTT-E or IgTT-1E and incubated for 72 hours. Viability was

assessed using the CellTiter-Glo luminescent assay (Promega, cat# G7570). For EGFR signaling studies, A431 cells were starved overnight in DMEM 1% FBS and then incubated for 4 hours in serum-free DMEM in the presence of 0.1 μM ctx, atz, IgTT-E or IgTT-1E, followed by 5 min incubation with 25 ng/ml of human EGF (MiltenyiBiotec, cat# 130-093-825). After stimulation, cells were lysed in Laemmli lysis buffer, separated under reducing conditions on 4–12% Tris-glycine gels, transferred to nitrocellulose membrane and incubated with the rabbit anti-human phosphor-EGFR (Tyr1068) mAb (clone D7A5; Cell Signaling Technology, cat# 3777) followed by incubation with an IRDye800CW-conjugated donkey anti-rabbit antibody (LI-COR Biosciences, cat# 925–32213). Simultaneously, anti- β -actin mouse mAb (Abcam, cat# ab8226) was added as a loading control, followed by IRDye680RD-conjugated donkey anti-mouse (LI-COR Biosciences, cat# 925–68072). Visualization and quantitative analysis of protein bands were carried out with the Odyssey system (LI-COR Biosciences).

PD-1/PD-L1 Blockade Bioassay

The PD-1/PD-L1 Bioassay (Promega, cat# J1250) was used following manufacturer's instructions. Briefly, 2.5×10^4 PD-L1 aAPC/CHO-K1 cells/well were seeded in 96-well white plates in DMEM 10% FBS and incubated overnight at 37 °C. Then, medium was removed and different final concentrations (400; 66.7; 6.67; 0.667 and 0.0667 nM) of atz, ctx, IgTT-E or IgTT-1E were added in 40 μl RPMI 1% FBS/well. Then, 1.25×10^5 Jurkat PD-1 cells/well were added in 40 μl RPMI 1% FBS/well and incubated 6 hours at 37 °C. Then, 80 μl of BioGlo Reagent (Promega, cat# G7941) were added and bioluminescence, as an indicator of activation, was measured in a Tecan Infinite F200 Fluorescence Microplate Reader (Life Sciences, Tecan).

ADCC reporter bioassay

The ADCC reporter Bioassay (Promega, cat# G7010) was used following manufacturer's instructions. Briefly, 1.2×10^4 CHO and CHO^{EGFR} cells/well were seeded in 96-well white plates in DMEM 10% FBS and incubated overnight at 37 °C. Then, medium was removed and different final concentrations (400, 66.7; 6.67; 0.667; 0.0667 nM) of atz, ctx or IgTT-1E were added in 25 μl RPMI 1% FBS/well. Then, 7.5×10^4 ADCC Jurkat^{CD16} effector cells/well were added in 25 μl RPMI 1% FBS and incubated 6 hours at 37 °C. Finally, 75 μl /well of BioGlo Reagent (Promega) were added and bioluminescence, as an indicator of ADCC activity, was measured in a Tecan Infinite F200 Fluorescence Microplate Reader.

Cytotoxicity assay

Peripheral blood mononuclear cells (PBMC) were isolated from peripheral blood of volunteer healthy donors by density gradient centrifugation using lymphoprep (Axis – Shield, cat# AXS-1114544). All donors provided written informed consent in accordance with the Declaration of Helsinki. For cytotoxicity assay, EGFR⁺ and PD-L1⁺ MDA-MB231^{Luc} and A549 cells

were co-cultured with freshly isolated PBMC at two different effector-to-target (E:T) ratios (5:1 and 10:1) in presence of atz, ctx, IgTT-1E or polyclonal control human IgG (6.67 nM). After 48 hours, cells were stained for 30 minutes at 4 °C with V450-conjugated anti-CD45 mAb (Becton Dickinson, cat# 560367) and 7-AAD (BD Biosciences, cat# 559925) in 50 μl of PBS 2% FBS using TruCount Absolute Counting Tubes (BD Biosciences, cat# 663028). Finally, the samples were diluted by adding 450 μl of PBS before proceeding to flow cytometry analysis. Cytotoxicity was determined by recording the residual live target cells (7AAD⁻ and CD45⁻).

NK cells degranulation assay

Degranulation of NK cells following *in vitro* stimulation was assessed by a flow cytometry-based assay. CHO, CHO^{PD-L1} and CHO^{EGFR} cells were seeded in 96-well U-bottom plates at 5×10^5 cells/well and co-cultured with 2.5×10^6 PBMC/well (5:1 E:T ratio) in the presence of monensin and PE-labeled anti-CD107a mAb (clone H4A3, BD Biosciences, cat# 555801). Then, IgTT-1E, ctx and atz were added to final concentrations of 6.67; 0.667 and 0.0667 nM. As basal degranulation control, PBMC were plated without target cells. A staining control well received neither degranulation stimuli nor the anti-CD107a mAb. After incubating for 4 hours, plates were centrifuged and cells were resuspended in PBS 0.5% FBS and stained with FITC-labeled anti-human CD3 (clone SK7, BD Biosciences, cat# 345763) and APC-labeled anti-human CD56 (clone B159, BD Pharmingen, cat# 555518) mAbs, and analyzed by a FACSCanto II Flow Cytometer (BD Biosciences). NK cells were identified as CD3⁻CD56⁺ events with light scatter characteristics of lymphocytes.

Mice

NOD.Cg-Prkdc^{SCID}IL2rg^{tm1Wjl}/SzJ (NSG, The Jackson Laboratory) female mice were housed under pathogen-free conditions with daily cycles of 12 hours light/12 hours darkness, and sterilized water and food were available *ad libitum*. All animal procedures conformed to European Union Directive 86/609/EEC and Recommendation 2007/526/EC, enforced in Spanish law under RD 1201/2005. Animal protocols were approved by the respective Ethics Committee of Animal Experimentation of the participant institutions (imas12 and Instituto Investigación Sanitaria Puerta de Hierro-Segovia de Arana); they were performed in strict adherence to the guidelines stated in the International Guiding Principles for Biomedical Research Involving Animals, established by the Council for International Organizations of Medical Sciences. The experimental study protocols were additionally approved by local government (PROEX 166/19). Mice were kept under anesthesia during all manipulations and all efforts were made to minimize suffering.

Therapeutic studies

MDA-MB-231^{Luc} cells were resuspended in 30% (v/v) matrigel (Corning, cat#356231) in PBS. Cells were injected directly into the second left mammary fat pad of NSG female mice (2×10^6

mouse), followed by an intraperitoneal (i.p.) injection of freshly isolated human PBMC (1×10^7 /mouse). Tumor growth was evaluated weekly by bioluminescence imaging. Mice were treated every three days with five intraperitoneal injections of PBS, atz, ctx or IgTT-1E (4 mg/kg), or atz/ctx (2 mg/kg) in combination. Mice weights were measured twice a week to monitor toxicity and animals were euthanized at any sign of distress and/or due to 20% of weight loss. For *in vivo* bioluminescence imaging, mice were anesthetized using inhaled isoflurane, injected intraperitoneally with 125 mg/kg D-luciferin (Promega, cat# E1605) dissolved in 200 μ l of sterile PBS. Animals were imaged 10 minutes after D-luciferin injection using the Bruker In-Vivo Xtreme (Bruker). The photon flux emitted by the luciferase-expressing cells was measured as an average radiance (photons/sec/cm²/sr). Imaging analysis was performed using Bruker Molecular Imaging Software (Bruker). At the end of the experiment anesthetized animals were sacrificed and the different organs (liver, spleen, and tumor) were rapidly harvested and processed. A549 cells (2×10^6 /mouse) resuspended in 30% (v/v) matrigel in PBS were implanted subcutaneously (s.c.) into the dorsal space of NSG mice, followed by an intraperitoneal injection of freshly isolated human PBMC (1×10^7 cells/mouse). Tumor growth was monitored by caliper measurements twice a week. Mice were treated every three days with five intraperitoneal injections of PBS, IgTT-1E (4 mg/kg) or atz/ctx (2 mg/kg) in combination. Mice weights were measured as described above. Mice were euthanized when the weight loss was $\geq 15\%$ compared to baseline, when tumor size reached a diameter of 1.0 cm in any dimension, when tumors ulcerated, or at any sign of distress.

Immunohistochemistry

Tumors from different treatment groups were collected at different times after implantation, fixed in 10% neutral buffered formalin (Sigma-Aldrich, cat#HT501128) for 48 hours and after extensive washing in PBS, tissues were embedded in paraffin. Four- μ m-thick sections were incubated with mouse mAbs listed in Table S2 on a BondTM Automated System (Leica Microsystems) according to the manufacturer's instructions. Nuclei were counter stained with Harris' hematoxylin. Whole digital slides were acquired with a slide scanner (AxioScan Z1, Zeiss), and total versus positive cells were automatically quantified (AxioVision 4.6 software package, Zeiss).

Statistical analysis

All plots were created using GraphPad Prism 9.0, which was also used to perform statistical analysis. In general, the *in vitro* experiments were done in triplicates and values are presented as mean \pm SD. Significant differences (*P* value) were identified using a two-tailed, unpaired Student's *t* test assuming a normal distribution, or a one-way analysis of variance (ANOVA), adjusted by Dunnett's test for multiple comparisons, as indicated. *P* values are shown in the corresponding figures. Two-way ANOVA was used to analyze experiments that evaluated the interaction of two variables, such as cell type and therapy, following multiple comparison testing using either Dunnett or Tukey, as appropriate. Mean tumor volumes are presented for

each group using a scatter plot as mean \pm SD. To assess the differences between treatment groups, *P* values were determined by one-way ANOVA adjusted by the Bonferroni correction for multiple comparison tests. Survival curves were estimated for each group using the Kaplan-Meier method and individual curves were analyzed by Log-rank (Mantel-Cox) test. Significant differences were calculated by comparing each group to the others.

Results

Generation and characterization of monospecific and bispecific IgTTs

In this study, we generated an EGFR-specific IgTT (Figure 1a) by fusing a V_{HH}-based monospecific TT (Figure 1b), consisting of three identical EGFR-specific V_{HH} (clone EGa1)¹³-TIE modules connected by two glycine-serine-based linkers on a single-chain molecule⁷, to the human IgG1 hinge-Fc regions (IgTT-E, Figure 1c). This antibody was further modified (Figure 1d) by replacing the N-terminal V_{HH} with an anti-PD-L1 scFv derived from *atezolizumab* (atz) (Figure 1e) to generate a PD-L1/EGFR bispecific IgTT (IgTT-1E, Figure 1f). The models presented in Figure 1 are snapshots of dynamic conformations in which the flexible connectors confer the V_{HH} and scFv binding domains variable distances and areas of influence around the Fc region. IgTT antibodies were purified from conditioned medium from stably transfected HEK-293 cells by Strep-Tactin affinity chromatography, and both molecules eluted as single peaks (Fig. a, b). Protein yields for IgTT-E and IgTT1E were 5.7 and 3.4 mg/L, respectively (Fig. S1a). SEC-MALS measurements for IgTT-E and IgTT-1E resulted in major symmetric peaks with molar masses of 227 and 240 kDa, respectively (Fig. S1a, b), close to the calculated values for each dimeric species in solution (202 and 223 kDa, respectively). In reducing SDS-PAGE, two main bands corresponding to the IgTT-E and IgTT-1E monomers can be identified (Fig. S1c). The smaller minority bands are most likely result of linker cleavage that does not disturb the structural organization of the molecule, as is evident from the observation of single peaks in SEC (Fig. S1a).

The binding of both IgTT antibodies to their cognate antigens was investigated using biolayer interferometry (BLI). Monospecific IgTT-E and bispecific IgTT-1E were found to bind immobilized human EGFR-Fc (EGFR) similarly to *cetuximab* (ctx) (Figure 2a,b), and IgTT-1E bound to human PD-L1-Fc (PD-L1) comparably to atz (Figure 2c). In all four interactions, less than 5% dissociation was measured during a period of 30 minutes, which was not sufficient to accurately determine the dissociation rate constant (KD). The upper bound for their dissociation rate constant is 3×10^{-5} /s and the lower bound for the half-life of their interactions is 7 hours. Therefore, these kinetic experiments demonstrate picomolar affinity or stronger for all the measured interactions, as is expected for bivalent and trivalent antibodies in an experiment which permits multivalent antigen binding, but do not determine precise KD values (Table S3). Additionally, after the binding of IgTT-1E and ctx to immobilized EGFR, the ability of the antibodies to simultaneously bind PD-L1 was investigated by additionally

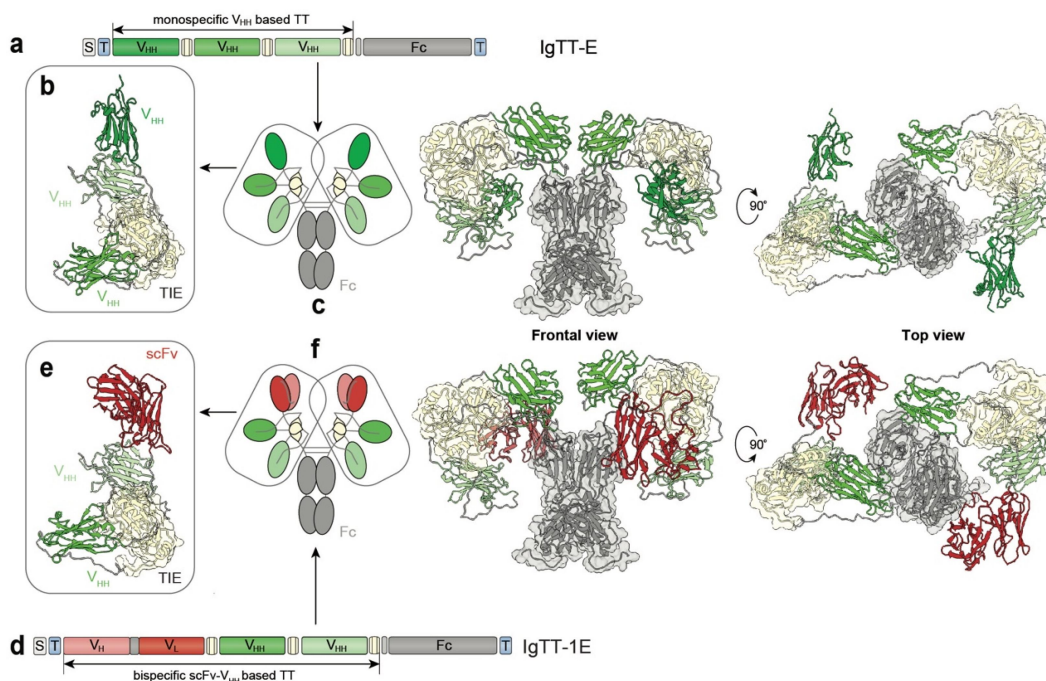


Figure 1. Molecular diagrams and models of the IgTT-E and IgTT-1E antibodies. Gene layout of the monospecific IgTT-E (a), bearing a signal peptide from oncostatin M (white box), three anti-EGFR V_{HH} (green boxes), three collagen-derived trimerization (TIE) domains (yellow boxes) flanked by peptide linkers and the Fc encoding element (gray boxes). N-terminal FLAG-Strep and C-terminal Myc-His tags (blue boxes) were appended for purification and immunodetection purposes. Schematic diagram showing the three-dimensional model of the TT (b), the molecular diagram and the three-dimensional modelizations of the IgTT-E, in front and top views (c). Gene layout of the bispecific IgTT-1E (d), bearing a signal peptide from oncostatin M (white box), one anti-PD-L1 scFv (red box) and two anti-EGFR V_{HH} genes (green boxes), three TIE domains (yellow boxes) flanked by peptide linkers and the Fc encoding element (gray boxes). N-terminal FLAG-Strep and C-terminal Myc-His tags (blue boxes). Schematic diagram showing the three-dimensional model of the TT (e), the molecular diagram and the three-dimensional modelizations of the IgTT-1E in front and top views (f).

associating the antibody-loaded biosensors with PD-L1 in solution. IgTT-1E, but not ctx, showed a clear simultaneous binding to PD-L1 while maintaining its interaction with EGFR (Figure 2d), further demonstrating its bispecificity and a lack of steric hindrance between its two cognate interactions. The ability of both antibodies to specifically detect human EGFR and PD-L1 in a cellular context was analyzed by flow cytometry, using ctx and atz as binding controls, and *trastuzumab* (tra) as negative control (Figure 2e). Furthermore, IgTT-1E demonstrated high stability in physiological-like conditions with no significant loss of binding activity after incubation at 37 °C for 96 hours in human serum (Figure S1d).

Effect of IgTT-1E on EGFR-mediated signaling and PD-1/PD-L1 blockade

We next studied the capacity of IgTT-1E to inhibit proliferation and EGFR phosphorylation using the ligand-competitive inhibitor ctx as a positive control and the anti-PD-L1 atz as a negative control. The epidermoid carcinoma A431 cell line is EGFR gene-amplified (1.2×10^6 sites/cell) and mostly depend on the EGFR/MAPK pathway for continuous proliferation^{18,19}. The anti-EGFR EgA1 V_{HH} binds an epitope close to junction of EGFR domains II/III, hindering the conformational changes in EGFR necessary for high-affinity ligand binding and receptor dimerization²⁰. As shown in Figure 3a, IgTT-E, IgTT-1E and ctx, but not atz, inhibited A431 cell proliferation in a dose-dependent manner ($P = <0.0001$, 0.0049 and <0.0001 ; respectively, for the highest doses of both IgTTs, vs. equimolar doses

of control antibody). The phosphorylation status of tyrosine 1068 (Tyr1068) was determined, as this tyrosine is the docking site for Grb2 and its phosphorylation allows the initiation of EGFR mitogenic cascade. Correspondingly, the inhibitory effect on cell proliferation correlated mechanistically with a reduction of EGFR phosphorylation (Figure 3b). The IgTT-1E efficiently blocked PD-1/PD-L1 interaction, as shown by the significant induction of luciferase activity on APC/CHO-K1 cells ($P < 0.0001$), similar to observed with the PD-L1 blocking antibody atz ($P < 0.0001$). In contrast, no PD-1/PD-L1 blocking activity was observed in the presence of ctx or IgTT-E (Figure 3c).

Determination of Fc-mediated effector functions

For measuring ADCC activity, Jurkat cells constitutively expressing human FcγRIIIa (CD16) on the cell surface and a luciferase reporter driven by a NFAT response element (Jurkat^{CD16}) were co-cultured with CHO cells stably expressing human EGFR (CHO^{EGFR}) or nontransfected CHO cells as negative control. As shown in Figure 3d, the activation of Jurkat^{CD16} cells by ctx and IgTT-1E in co-cultures with CHO^{EGFR} cells led to a significant increase in luciferase activity ($P < 0.0001$ and $P = 0.0074$, respectively). In the absence of EGFR-mediated interactions (co-cultures with nontransfected CHO cells), ctx and IgTT-1E showed no induction over untreated Jurkat^{CD16} cells (Figure 3d). Similarly, atz showed no activation in co-cultures with CHO^{EGFR} or CHO cells (Figure 3d). The atz Fc region has

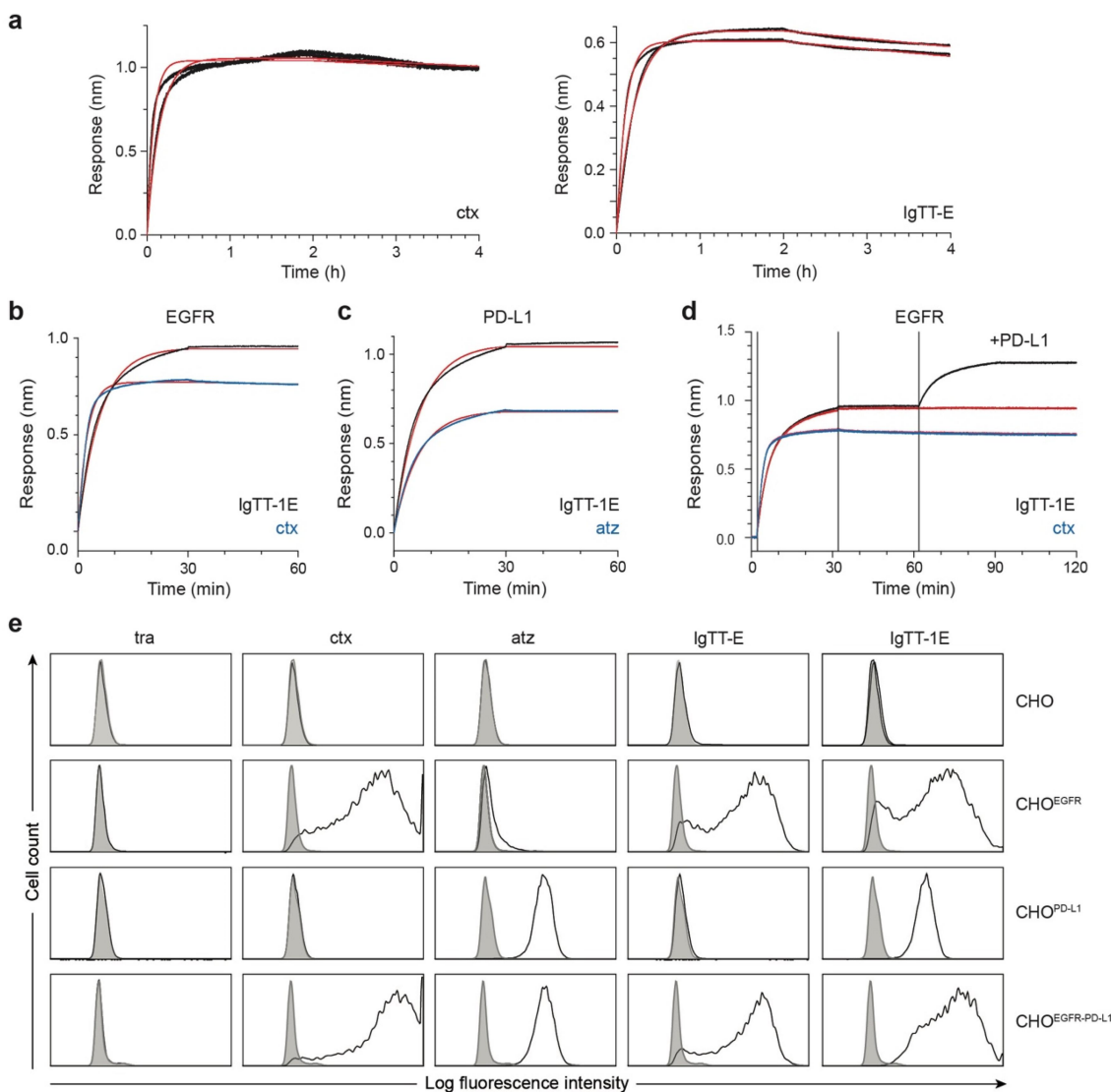


Figure 2. Binding characteristics of mono- and bispecific IgTT antibodies to EGFR, PD-L1, and both antigens simultaneously. (a) BLI-derived sensorgrams (in black) for the interaction between cetuximab (ctx) or IgTT-E and immobilized human EGFR-Fc. (b) Human EGFR-Fc was immobilized onto biosensors and 10 nM of either the IgTT-1E (black trace) or ctx (blue trace) was associated for 30 minutes, followed by 30 minutes of dissociation in buffer only. (c) as in the previous panel, binding to immobilized human PD-L1-Fc was investigated using atezolizumab (atz, blue trace) as a comparison antibody. The results of fitting to a 1:1 binding model are shown as red traces. Kinetic rate parameters from fitting are given in Table S3. A single experimental sensorgram of each antibody is shown; duplicate biosensors were included in the experiment and showed negligible variation. (d) Simultaneous binding to both immobilized human EGFR-Fc and human PD-L1-Fc in solution was demonstrated for IgTT-1E (black trace) but not ctx (blue trace). Human EGFR-Fc-coated biosensors were loaded with either IgTT-1E or ctx (as in the panel b), after which biosensors were immersed in 20 nM of human PD-L1-Fc or kept in buffer (red trace). (e) The binding to human EGFR and PD-L1 on the cell surface of CHO, CHO^{EGFR}, CHO^{PD-L1} and CHO^{EGFR-PD-L1} cells by trastuzumab (tra), ctx, atz, IgTT-E and IgTT-1E at 6.67 nM was measured by FACS. Cells incubated with PE-conjugated isotype control mAb are shown as gray-filled histogram. The y-axis shows the relative cell number, and the x-axis represents the intensity of fluorescence expressed on a logarithmic scale.

been engineered to reduce binding to Fcγ receptors and minimize ADCC^{21,22}. EGFR⁺PD-L1⁺ cancer cells (MDA-MB231 or A549) were co-cultured with human PBMC at two different E:T ratios (5:1 and 10:1) in the presence of atz, ctx, IgTT-1E or control human IgG (6.67 nM). A significant decrease in the residual live target cells was observed with IgTT-1E and ctx compared to atz and control IgG at both E:T ratios. IgTT-1E eliminated nearly 55% of the A549 cells and 70% of the MDA-MD23^{Luc} cells at the highest E:T ratio (Figure 3e). Furthermore, the IgTT-1E-mediated degranulation by NK cells was studied after co-culturing CHO and CHO^{EGFR} cells with PBMC at a 5:1 E:T ratio in the presence of different antibody concentrations. Both ctx and IgTT-1E increased CD107a cell surface expression

compared to PBMC co-cultured CHO^{EGFR} cells in the presence of atz. No changes in CD107a cell expression were detected when PBMC were co-cultured with CHO cells (Figure 3f, Figure. S2 and Table S4).

Therapeutic effect of IgTT-1E in vivo

The therapeutic potential of IgTT-1E was first investigated in PBMC-driven humanized NSG mice bearing human MDA-MB-231 TNBC CDXs. MDA-MB-231^{Luc} cells were injected into the second right mammary fat pad (MFP) and human PBMC intraperitoneally (i.p.). Mice were treated every three days for five i.p. injections in total, atz, ctx, IgTT-1E or the atz/ctx combination (combo) (Figure 4a). IgTT-1E monotherapy reduced tumor

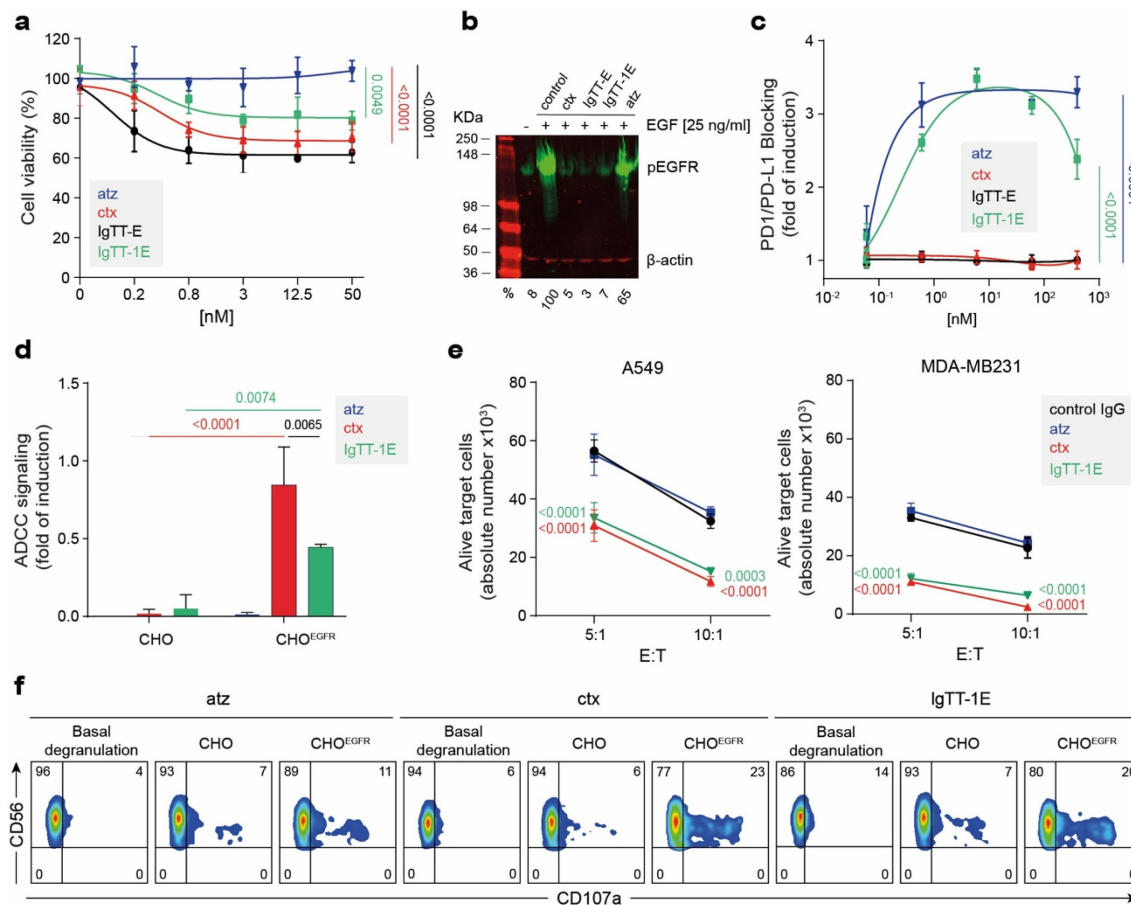


Figure 3. IgTT-1E reduces cell proliferation and induces cytotoxicity. (a) Inhibition of A431 cell proliferation through blocking of EGF/EGFR signaling. The cells were treated with the indicated doses of IgTT-E, IgTT-1E, ctx (positive control) or atz (negative control). Viable cells after 72 hours of treatment were plotted relative to untreated controls. Results are expressed as a mean \pm SD ($n = 3$). Significance was measured by one-way ANOVA with Dunnett's multiple comparisons test. (b) Inhibition of EGFR phosphorylation was assessed by western blotting. After pre-incubation with 50 nM of each antibody for 4 hours, cells were stimulated for 5 minutes with EGF or vehicle. Using the β -actin as load and signal control, the percentages of each phosphorylation band with respect to the positive control were calculated. (c) PD-1/PD-L1 blockade bioassay assesses the inhibitory activities of PD-L1 blocking antibody IgTT-1E. Y-axis represents reporter gene fold induction. Ctx was used as negative control and atz as positive control. Results are expressed as mean \pm SD ($n = 3$). Significance was measured by one-way ANOVA with Dunnett's multiple comparisons test. (d) ADCC reporter bioassay response to ctx, atz and IgTT-1E, using ADCC bioassay effector Jurkat^{CD16} cells against CHO and CHO^{EGFR} target cells. Target cells were incubated with ctx (positive control), atz (negative control) and IgTT-1E followed by addition of ADCC bioassay effector cells at a 6:1 E:T ratio. After 6 hours of cocultivation at 37°C Bio-Glo™ Luciferase Assay Reagent was added for luminescence determination. Data shown represent the mean \pm standard deviation of triplicates. Data are presented as the mean \pm SD ($n = 3$). Quantification shown as mean \pm SD, ($n = 3$). Significance was determined by two-way ANOVA with Tukey's multiple comparisons test. (e) The number of alive (7AAD⁻) target A549 and MDA-MB231 cells determined after 48 hour co-culture with PBMC cells at 5:1 and 10:1 E:T ratios in presence of control human IgG, atz, ctx and IgTT-1E. Results are shown as mean \pm SD ($n = 3$). Significance was determined by two-way ANOVA with Dunnett's multiple comparisons test. (f) Human PBMC were incubated with ctx, atz and IgTT-1E (0.667 nM) for 4 hours prior to flow cytometry evaluation of CD107a cell surface expression on NK cells, gated as CD3⁻CD56⁺ cells.

bioluminescence in 4 out of 5 treated mice, similar to what was found in the groups receiving atz or combination therapy (Figure 4b,c). Consistent with these antitumor results, a significant overall survival benefit was observed for the mice that had been treated with atz ($P = 0.0122$) or IgTT-1E ($P = 0.0054$) compared to ctx (Figure 4d). To further validate the antitumor activity of IgTT-1E, we performed a second study with PBMC-driven humanized NSG mice bearing human A549 lung cancer CDXs. When tumors reached approximately 0.2 cm in diameter, mice were randomized into groups with similar mean tumor sizes and SDs and treated every three days for five i.p. injections in total of IgTT-1E or the atz/ctx combination (Figure 4e). IgTT-1E monotherapy was able to reduce tumor growth by approximately 85% ($P = 0.0001$), while the

combination therapy showed an approximately 90% tumor growth reduction ($P = 0.0001$) (Figure 4f). There were no significant body weight decreases in any group (Figure 4g). In both treatment groups, inhibition of tumor growth was associated with significantly increased numbers of intratumoral CD8⁺ T cells (Figure 4h, i and Figure S3), while no CD56⁺ NK cells were detected on tumor tissues (Fig. S4).

Discussion

In recent years, new cancer immunotherapy strategies have been developed based on the generation of bsAb with improved properties over conventional mAbs^{8,12,14,23}. Currently, there are five FDA-approved bsAbs for cancer

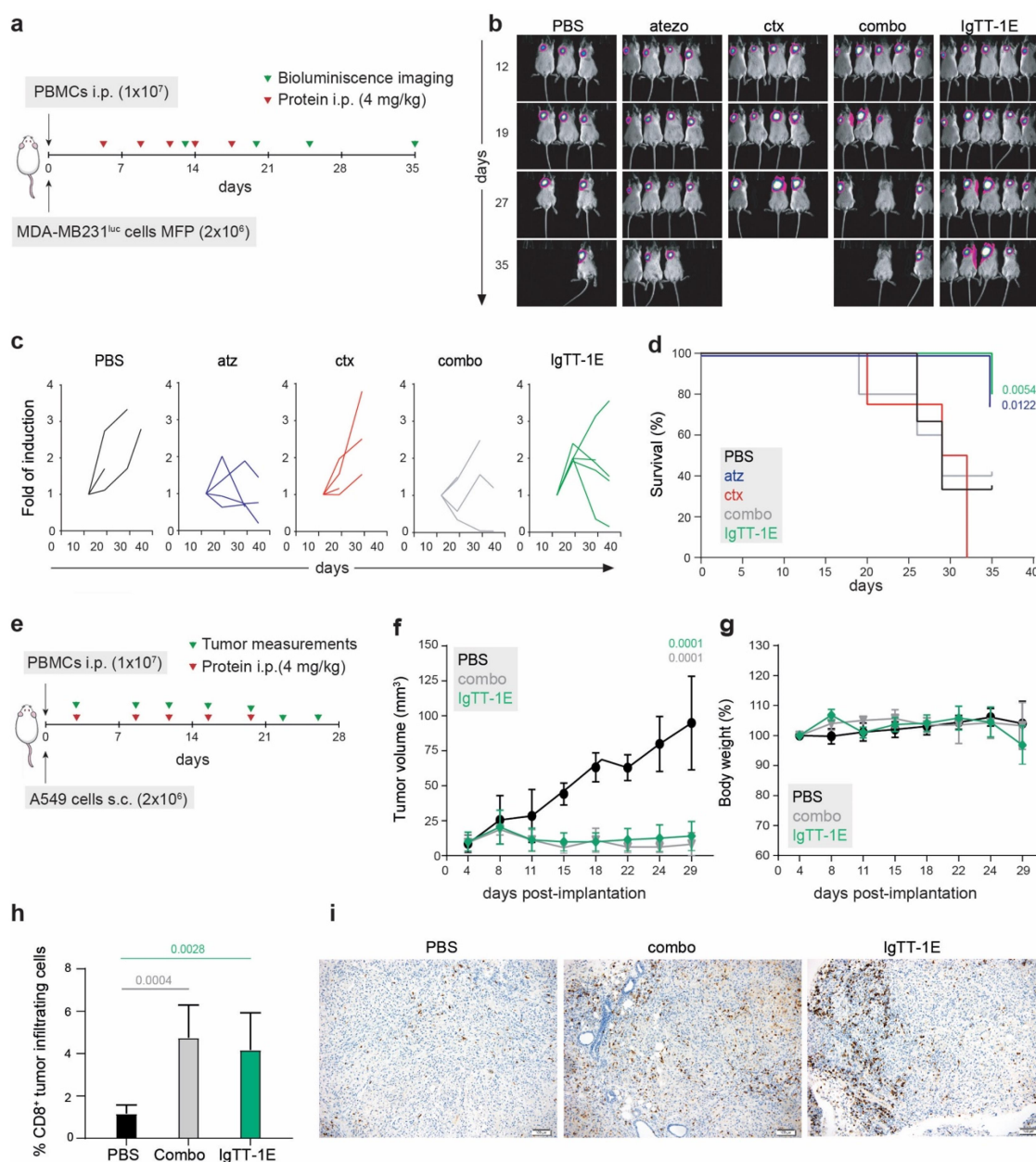


Figure 4. IgTt-1E treatment promoted significant tumor growth inhibition in NSG mouse models. (a) Timeline of experimental design. MDA-MB-231^{Luc} cells were implanted into the right mammary fat pad (MFP) of NSG mice, and human PBMC were injected intraperitoneally (i.p.). Mice were treated with five i.p. injections of PBS, atz, ctx, atz + ctx (combo) or IgTt-1E. (b) Weekly bioluminescence imaging showing tumor progression. (c) Quantification of tumor burden (as bioluminescence fold induction from each mouse) at the indicated time points. (d) Kaplan-Meier plot of survival data. (e) Timeline of experimental design. NSG mice were subcutaneously (s.c.) inoculated with A549 tumor cells and i.p. with human PBMC, follow by five i.p. injections of PBS, atz + ctx combo or IgTt-1E. Tumor progression was monitored weekly by diameter measuring. (f) Average tumor volume growth in each mice group. Data are presented as the mean \pm SD. Significance was determined by one-way ANOVA adjusted by the Bonferroni correction for multiple comparison test. (g) Change in mouse body weight over time for each group. (h) Quantitative analysis of intratumoral CD8⁺ T cells in paraffin-embedded mouse tumor tissue (PBS $n = 4$, combo $n = 6$, IgTt-1E $n = 6$) by immunohistochemistry. Data were calculated as percentage of CD8⁺ versus total cell number and presented as mean \pm SD. Significance was measured by one-way ANOVA with Dunnett's multiple comparisons test. (i) Immunohistochemical staining for CD8 of representative tissue slides from the tumor of mice treated with PBS, atz + ctx combo or IgTt-1E. Scale bars (100 μ m) are shown.

treatment, *blinatumomab* for acute B cell lymphoblastic leukemia, *amivantamab-vmjw* for NSCLC, *tebentafusp-tebn* for uveal melanoma, *mosunetuzumab-axgb* for follicular lymphoma, and *teclistamab-cqyv* for multiple myeloma^{12,15}, and more than 120 candidates are in clinical development¹⁶. Despite advances in antibody engineering, the generation of IgG-like bsAb remains challenging when the antigen-binding sites are Fab-like with the variable regions of both the heavy

chain (V_H) and light chain (VL), as this makes it difficult to obtain functional bsAb from the random assembly of ten possible H_2L_2 combinations (this is commonly referred to as the chain-association issue)^{17–20}. Therefore, to overcome this and other limitations a wide variety of antibody engineering strategies have been developed in recent years^{9,23}. Symmetric bsAbs are generated by the assembly of antibodies with unmodified heavy chain (HC) constant (C_H) regions^{21,23}. Most

symmetric bsAbs in clinical development are bulky molecules with tetravalent (2 + 2) designs in which extra antibody fragments are fused to homodimeric antibody molecules^{22,23}. Otherwise, the generation of asymmetric IgG-like bsAbs continues to be challenging because two critical issues need to be simultaneously addressed: the heterodimerization of two different HC chains and the discrimination between the two L/H chain interactions^{21,23,24}. Correct HC heterodimerization is facilitated using engineering strategies such as knobs-into-holes and crossMAb technologies^{23,25–28}. However, most of these strategies employ multiple mutations within the C_H domains, which can negatively affect the favorable properties associated with native Fc regions, such as high stability and solubility, as well as increasing their immunogenicity²⁹.

Here, we generated a novel PD-L1/EGFR IgG-like bsAb by novel antibody engineering that solves some of the problems associated with bispecific heterodimeric IgG antibody generation, such as the chain-association issue^{17–20}. The IgTT format is based on the fusion of a mono or multispecific TT⁷ with the human IgG1 hinge and Fc region, generating a hexavalent IgG-like antibody capable of bivalently recognizing up to three different antigens. We initially generated a monospecific IgTT molecule targeting EGFR, a well-characterized TAA that is the one of the most commonly overexpressed membranous oncogenic protein in epithelial cancers³⁰. In addition, we have demonstrated the suitability of the IgTT format for dual-targeting strategies combining TAA-recognition with an ICB, in a single molecule. Both IgTT molecules specifically bind to their targeted antigens, and the IgTT-1E displayed simultaneous binding to both antigens. As previously described, the interaction of EGal V_{HH} with EGFR inhibited EGFR phosphorylation and cell proliferation^{7,11,31}. Furthermore, the bispecific IgTT-1E efficiently blocked PD-1/PD-L1 interaction and promoted efficient EGFR-mediated ADCC.

The combined PD-L1 and EGFR targeting by bsAbs has been shown to enhance PD-L1 blockade selectively in the TME, due to EGFR overexpression in cancer cells, and to reduce potential off-tumor binding to PD-L1-expressing normal cells³². Because of its distinctive properties including tetravalent binding to EGFR, bivalent binding to PD-L1, and a molecular mass similar to IgG, the IgTT-1E is expected to demonstrate improved tumor localization compared to previously generated bsAbs. Furthermore, EGFR overexpression and activation promotes PD-L1 expression by cancer cells³³. Therefore, EGFR is a particularly suitable TAA for the development of next-generation bispecific ICB. Compared to other IgG-like bsAbs simultaneously targeting EGFR and PD-L1^{34,35}, the IgTT-1E is based on an IgG1 wild-type homodimeric Fc region retaining ADCC activity as in Li et al.³⁵. Indeed, IgTT-1E might induce ADCC activity in the intratumoral space reducing the tumor burden and priming immune responses, as has been shown with *cetuximab*³⁶. The concomitant presence of PD-L1 blocking domains in the same spatial location would be essential to overcome immunosuppressive counter-

mechanisms in the TME and fully mobilize the adaptive and innate immunity against tumor cells. In addition, the presence of a functional Fc region in the molecule, as in the case of *cetuximab*, has been shown to induce NK cell-dendritic cell (DC) crosstalk, promoting DC maturation and leading to CD8⁺ T cell priming^{37–47}. Therefore, IgTT-1E may provide sustained CD8⁺ T activity by inducing NK-DC crosstalk and blocking PD-1/PD-L1 interaction, leading to a more prolonged function of tumor-infiltrating lymphocytes.

Acknowledgments

We thank Carlos Alfonso for help with SEC-MALS experiments.

Disclosure statement

M.C., R.N., and O.H. are all employees of Leadartis. L.A.-V. and L.S. are co-founders of Leadartis. The remaining authors declare no competing interests.

Funding

L.A.-V. was supported by grants from the MCIN/AEI/10.13039/501100011033 (PID2020-117323RB-I00 and PDC2021-121711-I00), the Instituto de Salud Carlos III (DTS20/00089), the CRIS Cancer Foundation (FCRIS-2021-0090), the Spanish Association Against Cancer (PROYE19084ALVA), the Fundación “La Caixa” (HR21-00761 project IL7R_LungCan) and the Fundación de Investigación Biomédica 12 de Octubre Programa Investiga (2022-0082). B.B. and L.S. were supported by grants PI20/01030 and PI19/00132 from the Instituto de Salud Carlos III (PI20/01030). FJB and MF-G were supported by grants PID2020-113225GB-I00 and PRE2018-085788 funded by MCIN/AEI/10.13039/501100011033. L.R.-P. was supported by a predoctoral fellowship from the Immunology Chair, Universidad Francisco de Vitoria/Merck. C. D.-A. was supported by a predoctoral fellowship from the MCIN/AEI/10.13039/501100011033 (PRE2018-083445). L.D.-A. was supported by a Rio Hortega fellowship from the Instituto de Salud Carlos III (CM20/00004). O.H. was supported by an industrial PhD fellowship from the Comunidad de Madrid (IND2020/BMD-17668). AE-L was supported industrial PhD fellowship from the Instituto de Salud Carlos III (IFI18/00045).

ORCID

Laura Rubio-Pérez  <http://orcid.org/0000-0002-2877-6092>
 Rodrigo Lázaro-Gorines  <http://orcid.org/0000-0002-6885-3486>
 Seandean L. Harwood  <http://orcid.org/0000-0003-4654-8832>
 Marta Compte  <http://orcid.org/0000-0002-7138-9266>
 Rocío Navarro  <http://orcid.org/0000-0002-0083-7711>
 Antonio Tapia-Galisteo  <http://orcid.org/0000-0002-0507-8435>
 Jaime Bonet  <http://orcid.org/0000-0001-5210-4387>
 Belén Blanco  <http://orcid.org/0000-0001-5085-7756>
 Simon Lykkemark  <http://orcid.org/0000-0001-8920-6926>
 Ángel Ramírez-Fernández  <http://orcid.org/0000-0002-3265-6878>
 Mariola Ferreras-Gutiérrez  <http://orcid.org/0000-0003-4421-3158>
 Carmen Domínguez-Alonso  <http://orcid.org/0000-0002-0446-9629>
 Laura Diez-Alonso  <http://orcid.org/0000-0002-9545-6910>
 Alejandro Segura-Tudela  <http://orcid.org/0000-0002-5506-0153>
 Francisco J. Blanco  <http://orcid.org/0000-0003-2545-4319>
 Cruz Santos  <http://orcid.org/0000-0001-5164-5050>
 José L. Rodríguez-Peralto  <http://orcid.org/0000-0002-6578-7153>
 Laura Sanz  <http://orcid.org/0000-0002-3119-3218>
 Luis Álvarez-Vallina  <http://orcid.org/0000-0003-3053-6757>

Ethics approval

All procedures involving animals were in accordance with the ethical standards of the corresponding institutional and regional/national committees.

Data availability statement

The datasets used and/or analyzed during the current study are available from the corresponding author [LA-V] on reasonable request.

Consent to participate

Informed consent was obtained from all participants included in the study.

References

- Mahoney KM, Rennert PD, Freeman GJ. Combination cancer immunotherapy and new immunomodulatory targets. *Nat Rev Drug Discov.* 2015;14:561–584. doi:10.1038/nrd4591.
- Sharpe AH, Pauken KE. The diverse functions of the PD1 inhibitory pathway. *Nat Rev Immunol.* 2018;18:153–167. doi:10.1038/nri.2017.108.
- Freeman GJ, Long AJ, Iwai Y, Bourque K, Chernova T, Nishimura H, Fitz LJ, Malenkovich N, Okazaki T, Byrne MC, et al. Engagement of the PD-1 immunoinhibitory receptor by a novel B7 family member leads to negative regulation of lymphocyte activation. *J Exp Med.* 2000;192:1027–1034. doi:10.1084/jem.192.7.1027.
- Wei SC, Duffy CR, Allison JP. Fundamental mechanisms of immune checkpoint blockade therapy. *Cancer Discov.* 2018;8:1069–1086. doi:10.1158/2159-8290.CD-18-0367.
- Morad G, Helmink BA, Sharma P, Wargo JA. Hallmarks of response, resistance, and toxicity to immune checkpoint blockade. *Cell.* 2021;184:5309–5337. doi:10.1016/j.cell.2021.09.020.
- Kubli SP, Berger T, Araujo DV, Siu LL, Mak TW. Beyond immune checkpoint blockade: emerging immunological strategies. *Nat Rev Drug Discov.* 2021;20:899–919. doi:10.1038/s41573-021-00155-y.
- Roskoski R. The ErbB/HER family of protein-tyrosine kinases and cancer. *Pharmacol Res.* 2014;79:34–74. doi:10.1016/j.phrs.2013.11.002.
- Levantini E, Maroni G, Del Re M, Tenen DG. EGFR signaling pathway as therapeutic target in human cancers. *Semin Cancer Biol.* 2022;85:253–275. doi:10.1016/j.semcancer.2022.04.002.
- Antibody therapeutics approved or in regulatory review in the EU or US [Internet]. The Antibody Society. [accessed 2023 March 1]. <https://www.antibodysociety.org/resources/approved-antibodies/>
- Cuesta AM, Sainz-Pastor N, Bonet J, Oliva B, Alvarez-Vallina L. Multivalent antibodies: when design surpasses evolution. *Trends Biotechnol.* 2010;28:355–362. doi:10.1016/j.tibtech.2010.03.007.
- Cuesta AM, Sánchez-Martín D, Blanco-Toribio A, Villate M, Enciso-Álvarez K, Álvarez-Cienfuegos A, Sainz-Pastor N, Sanz L, Blanco FJ, Álvarez-Vallina L. Improved stability of multivalent antibodies containing the human collagen XV trimerization domain. *MAbs.* 2012;4:226–232. doi:10.4161/mabs.4.2.19140.
- Lazarovici P, Lelkes PI. Pardaxin induces exocytosis in bovine adrenal medullary chromaffin cells independent of calcium. *J Pharmacol Exp Ther.* 1992;263:1317–1326.
- Alvarez-Cienfuegos A, Nuñez-Prado N, Compte M, Cuesta AM, Blanco-Toribio A, Harwood SL, Villate M, Merino N, Bonet J, Navarro R, et al. Intramolecular trimerization, a novel strategy for making multispecific antibodies with controlled orientation of the antigen binding domains. *Sci Rep.* 2016;6:28643. doi:10.1038/srep28643.
- Saphire EO, Parren PW, Pantophlet R, Zwick MB, Morris GM, Rudd PM, Dwek RA, Stanfield RL, Burton DR, Wilson IA. Crystal structure of a neutralizing human IGG against HIV-1: a template for vaccine design. *Science.* 2001;293:1155–1159. doi:10.1126/science.1061692.
- Berman HM, Westbrook J, Feng Z, Gilliland G, Bhat TN, Weissig H, Shindyalov IN, Bourne PE. The Protein Data Bank. *Nucleic Acids Res.* 2000;28:235–242. doi:10.1093/nar/28.1.235.
- Altschul SF, Gish W, Miller W, Myers EW, Lipman DJ. Basic local alignment search tool. *J Mol Biol.* 1990;215:403–410. doi:10.1016/S0022-2836(05)80360-2.
- Liu S, Miersch S, Li P, Bai B, Liu C, Qin W, Su J, Huang H, Pan J, Sidhu SS, et al. A synthetic human antibody antagonizes IL-18R β signaling through an allosteric mechanism. *J Mol Biol.* 2020;432:1169–1182. doi:10.1016/j.jmb.2020.01.012.
- Janmaat ML, Kruyt FAE, Rodriguez JA, Giaccone G. Response to epidermal growth factor receptor inhibitors in non-small cell lung cancer cells: limited antiproliferative effects and absence of apoptosis associated with persistent activity of extracellular signal-regulated kinase or Akt kinase pathways. *Clin Cancer Res.* 2003;9:2316–2326.
- Meira DD, Nóbrega I, de Almeida VH, Mororó JS, Cardoso AM, Silva RLA, Albano RM, Ferreira CG. Different antiproliferative effects of matuzumab and cetuximab in A431 cells are associated with persistent activity of the MAPK pathway. *Eur J Cancer.* 2009;45:1265–1273. doi:10.1016/j.ejca.2008.12.012.
- Schmitz KR, Bagchi A, Roovers RC, van Bergen En Henegouwen PMP, Ferguson KM. Structural evaluation of EGFR inhibition mechanisms for nanobodies/VHH domains. *Structure.* 2013;21:1214–1224. doi:10.1016/j.str.2013.05.008.
- Deng R, Bumbaca D, Pastuskovas CV, Boswell CA, West D, Cowan KJ, Chiu H, McBride J, Johnson C, Xin Y, et al. Preclinical pharmacokinetics, pharmacodynamics, tissue distribution, and tumor penetration of anti-PD-L1 monoclonal antibody, an immune checkpoint inhibitor. *MAbs.* 2016;8:593–603. doi:10.1080/19420862.2015.1136043.
- Shah NJ, Kelly WJ, Liu SV, Choquette K, Spira A. Product review on the Anti-PD-L1 antibody atezolizumab. *Human Vacc Immunother.* 2018;14:269–276. doi:10.1080/21645515.2017.1403694.
- Harwood SL, Alvarez-Cienfuegos A, Nuñez-Prado N, Compte M, Hernández-Pérez S, Merino N, Bonet J, Navarro R, Van Bergen En Henegouwen PMP, Lykkemark S, et al. ATTACK, a novel bispecific T cell-recruiting antibody with trivalent EGFR binding and monovalent CD3 binding for cancer immunotherapy. *Oncoimmunology.* 2017;7:e1377874. doi:10.1080/2162402X.2017.1377874.
- Surowka M, Schaefer W, Klein C. Ten Years in the making: application of CrossMab technology for the development of therapeutic bispecific antibodies and antibody fusion proteins. *MAbs.* 2021;13:1967714. doi:10.1080/19420862.2021.1967714.
- Blanco B, Domínguez-Alonso C, Alvarez-Vallina L. Bispecific immunomodulatory antibodies for cancer immunotherapy. *Clin Cancer Res.* 2021;27:5457–5464. doi:10.1158/1078-0432.CCR-20-3770.
- Esfandiari A, Cassidy S, Webster RM. Bispecific antibodies in oncology. *Nat Rev Drug Discov.* 2022;21:411–412. doi:10.1038/d41573-022-00040-2.
- Henricks LM, Schellens JHM, Huitema ADR, Beijnen JH. The use of combinations of monoclonal antibodies in clinical oncology. *Cancer Treat Rev.* 2015;41:859–867. doi:10.1016/j.ctrv.2015.10.008.
- Progress in overcoming the chain association issue in bispecific heterodimeric IgG antibodies - PubMed [Internet]. [accessed 2022 December 19]. <https://pubmed.ncbi.nlm.nih.gov/22925968/>
- Rath T, Baker K, Dumont JA, Peters RT, Jiang H, Qiao S-W, Lencer WI, Pierce GF, Blumberg RS. Fc-fusion proteins and FcRn: structural insights for longer-lasting and more effective therapeutics. *Crit Rev Biotechnol.* 2015;35:235–254. doi:10.3109/07388551.2013.834293.
- Clarke SC, Ma B, Trinklein ND, Schellenberger U, Osborn MJ, Ouisse L-H, Boudreau A, Davison LM, Harris KE, Ugamraj HS, et al. Multispecific antibody development platform based on

- human heavy chain antibodies. *Front Immunol.* 2019;9:3037. doi:10.3389/fimmu.2018.03037.
31. Labrijn AF, Meesters JI, de Goeij BECG, van den Bremer ETJ, Neijssen J, van Kampen MD, Strumane K, Verploegen S, Kundu A, Gramer MJ, et al. Efficient generation of stable bispecific IgG1 by controlled Fab-arm exchange. *Proc Natl Acad Sci U S A.* 2013;110:5145–5150. doi:10.1073/pnas.1220145110.
 32. Wu Y, Yi M, Zhu S, Wang H, Wu K. Recent advances and challenges of bispecific antibodies in solid tumors. *Exp Hematol Oncol.* 2021;10:56. doi:10.1186/s40164-021-00250-1.
 33. Brinkmann U, Kontermann RE. The making of bispecific antibodies. *MAbs.* 2017;9:182–212. doi:10.1080/19420862.2016.1268307.
 34. Marvin JS, Zhu Z. Recombinant approaches to IgG-like bispecific antibodies. *Acta Pharmacol Sin.* 2005;26:649–658. doi:10.1111/j.1745-7254.2005.00119.x.
 35. Merchant AM, Zhu Z, Yuan JQ, Goddard A, Adams CW, Presta LG, Carter P. An efficient route to human bispecific IgG. *Nat Biotechnol.* 1998;16:677–681. doi:10.1038/nbt0798-677.
 36. Labrijn AF, Janmaat ML, Reichert JM, Parren PWHI. Bispecific antibodies: a mechanistic review of the pipeline. *Nat Rev Drug Discov.* 2019;18:585–608. doi:10.1038/s41573-019-0028-1.
 37. Spiess C, Zhai Q, Carter PJ. Alternative molecular formats and therapeutic applications for bispecific antibodies. *Mol Immunol.* 2015;67:95–106. doi:10.1016/j.molimm.2015.01.003.
 38. J-H H, Kim J-E, Kim Y-S. Immunoglobulin Fc heterodimer platform technology: from design to applications in therapeutic antibodies and proteins. *Front Immunol.* 2016;7:394. doi:10.3389/fimmu.2016.00394.
 39. Ridgway JB, Presta LG, Carter P. ‘Knobs-into-holes’ engineering of antibody CH3 domains for heavy chain heterodimerization. *Protein Eng.* 1996;9:617–621. doi:10.1093/protein/9.7.617.
 40. Nuñez-Prado N, Compte M, Harwood S, Álvarez-Méndez A, Lykkemark S, Sanz L, Álvarez-Vallina L. The coming of age of engineered multivalent antibodies. *Drug Discov Today.* 2015;20:588–594. doi:10.1016/j.drudis.2015.02.013.
 41. Thomas R, Weihua Z. Rethink of EGFR in cancer with its kinase independent function on board. *Front Oncol.* 2019;9:800. doi:10.3389/fonc.2019.00800.
 42. Akbay EA, Koyama S, Carretero J, Altabel A, Tchaicha JH, Christensen CL, Mikse OR, Cherniack AD, Beauchamp EM, Pugh TJ, et al. Activation of the PD-1 pathway contributes to immune escape in EGFR-driven lung tumors. *Cancer Discov.* 2013;3:1355–1363. doi:10.1158/2159-8290.CD-13-0310.
 43. Chen N, Fang W, Zhan J, Hong S, Tang Y, Kang S, Zhang Y, He X, Zhou T, Qin T, et al. Upregulation of PD-L1 by EGFR activation mediates the immune escape in EGFR-Driven NSCLC: implication for optional immune targeted therapy for NSCLC patients with EGFR mutation. *J Thorac Oncol.* 2015;10:910–923. doi:10.1097/JTO.0000000000000500.
 44. Koopmans I, Hendriks D, Samplonius DF, Ginkel RJ, Heskamp S, Wierstra PJ, Bremer E, Helfrich W. A novel bispecific antibody for EGFR-directed blockade of the PD-1/PD-L1 immune checkpoint. *Oncoimmunology.* 2018;7:e1466016. doi:10.1080/2162402X.2018.1466016.
 45. Li L, Deng L, Meng X, Gu C, Meng L, Li K, Zhang X, Meng Y, Xu W, Zhao L, et al. Tumor-targeting anti-EGFR x anti-PD1 bispecific antibody inhibits EGFR-overexpressing tumor growth by combining EGFR blockade and immune activation with direct tumor cell killing. *Transl Oncol.* 2021;14:100916. doi:10.1016/j.tranon.2020.100916.
 46. Ferris RL, Lenz H-J, Trotta AM, García-Foncillas J, Schulten J, Audhuy F, Merlano M, Milano G. Rationale for combination of therapeutic antibodies targeting tumor cells and immune checkpoint receptors: harnessing innate and adaptive immunity through IgG1 isotype immune effector stimulation. *Cancer Treat Rev.* 2018;63:48–60. doi:10.1016/j.ctrv.2017.11.008.
 47. Srivastava RM, Lee SC, Andrade Filho PA, Lord CA, Jie H-B, Davidson HC, López-Albaitero A, Gibson SP, Gooding WE, Ferrone S, et al. Cetuximab-activated natural killer and dendritic cells collaborate to trigger tumor antigen-specific T-cell immunity in head and neck cancer patients. *Clin Cancer Res.* 2013;19:1858–1872. doi:10.1158/1078-0432.CCR-12-2426.